AIP | Journal of Applied Physics

Magnetic interaction and conical self-reorganization of aligned tin oxide nanowire array under field emission conditions

Samad Bazargan, Joseph P. Thomas, and K. T. Leung

Citation: J. Appl. Phys. **113**, 234305 (2013); doi: 10.1063/1.4811234
View online: http://dx.doi.org/10.1063/1.4811234
View Table of Contents: http://jap.aip.org/resource/1/JAPIAU/v113/i23
Published by the AIP Publishing LLC.

JOURNAL OF APPLIED PHYSICS **113**, 234305 (2013)

Magnetic interaction and conical self-reorganization of aligned tin oxide nanowire array under field emission conditions

Samad Bazargan, Joseph P. Thomas, and K. T. Leung[a)]
WATLab and Department of Chemistry, University of Waterloo, Waterloo, Ontario N2L 3G1, Canada

(Received 3 March 2013; accepted 30 May 2013; published online 18 June 2013)

Magnetic interactions are induced between non-magnetic, vertically aligned tin dioxide nanowires under field-emission conditions. Vertically aligned nanowires of tin dioxide are synthesized along the [100] direction by pulsed laser deposition of an epitaxial (200) seed layer on c-cut sapphire substrates followed by vapor-liquid-solid growth using catalyst-assisted pulsed laser deposition method. Due to the dense arrangement of the vertically aligned ultra-long nanowires deposited in this study, magnetic interactions between the nanowires carrying parallel currents become significant within 1 μm radius and lead to their self-reorganization into conical tipi structures under field emission conditions. Optimization of the aerial density of the emission tips and reduction in the field screening effects upon self-reorganization of the nanowire array can account for the large field enhancement factor of 2.6×10^4 at low turn-on field of 3 V/μm. © *2013 AIP Publishing LLC*. [http://dx.doi.org/10.1063/1.4811234]

INTRODUCTION

Transparent conducting oxides (TCOs) are of great scientific and technological importance for their numerous applications in optoelectronics, photovoltaics, display, sensing, and catalysis. These TCO materials, including ZnO, SnO_2, In_2O_3, and TiO_2, exhibit a rich variety of morphologies at the nanoscale, among which quasi one-dimensional (1D) nanostructures are of special interest. In addition to providing a large surface area, these 1D nanostructures offer a superior charge transport medium due to reduced grain boundary scattering and charge transport barriers in their single crystalline structure. These nanostructures have shown promising performance as field-effect transistors,[1] chemical sensors,[2] optical waveguides,[3] lasers,[4] photodiodes, and field-emitters.[5] Synthesis of vertically aligned nanowires (NWs) of TCO materials with control on their length and density can provide great advantages in the application of these 1D nanomaterials in photovoltaics, photonics, 3D hierarchical device structures, and field-emission displays. Among the most studied TCO nanostructures, 1D nanostructures of SnO_2 (TO) have been found to exhibit excellent performance as gas,[2] pH and biomolecule sensors,[6] subwavelength optical waveguides,[3] field-effect transistors,[1] and field emitters.[7,8] Various methods have been used for growing 1D TO nanostructures, where thermal evaporation[9] is one of the most widely used techniques. Recently, we reported the use of a catalyst-assisted pulsed laser deposition (CPLD) method for depositing a variety of TO nanostructures including nanobelts and nanowires.[10] Thermal evaporation and laser ablation synthesis could, to date, only produce 1D TO nanostructures with random growth orientations on amorphous quartz[11,12] or alumina substrates[13] or tube walls of the furnaces.[9] Our most recent work on the CPLD growth of 1D TO nanostructures directly on oxidized-Si and $Al_2O_3(0001)$ substrates further shows that while it is possible to control the preferred crystalline growth axis by pinning the nanostructures to the substrate, the growth direction remains random.[14]

In the present work, we use the PLD method to first deposit an epitaxial seed layer of TO on an $Al_2O_3(0001)$ substrate before growing 1D nanostructures by CPLD. This new technique has allowed us to grow, for the first time, vertically aligned TO nanowires epitaxially with square cross sections of ca. 70×70 nm^2 and ultra-long lengths of up to 15 μm. Moreover, the control on density, length, and alignment of the nanowires enables us to demonstrate the significant induced magnetic interaction between non-magnetic nanowires during the field emission (FE) measurements. This magnetic attraction is shown to lead to modifications in the morphology and field emission properties of the nanowire array.

EXPERIMENTAL DETAILS

PLD experiments are performed by using a KrF excimer laser to deliver an energy of 350 mJ per pulse at 5 Hz to ablate a TO target in a high-vacuum chamber with the base pressure of 8×10^{-8} Torr. As-purchased epi-polished $Al_2O_3(0001)$ substrates are treated with aqua regia for 10 min and then sonicated in Millipore water, acetone, and isopropanol to remove any organic and inorganic contaminants. With the target-to-substrate distance kept at 40–50 mm, the seed layer is then deposited onto the substrate at 650–700 °C in oxygen ambient of 400 mTorr for 30 min. Nanowire (1–15 μm long) deposition promoted by gold nanoisland (GNI) catalysts is carried out in conditions similar to those described in our recent studies[10] at 500 °C and argon pressure of 400 mTorr for 40–60 min. Morphology of the samples is examined by using a Zeiss Orion Plus helium ion microscope and a Zeiss Ultra Plus field-emission scanning electron microscope. Transmission electron microscopy studies are performed by using a JOEL 2010F microscope on

a)E-mail: tong@uwaterloo.ca

nanowires scraped off from the substrate and transferred onto a lacey carbon grid. Epitaxial growth and average crystallinity of the samples are examined by using a PANalytical MRD X'pert Pro diffractometer with a Cu Kα source. Symmetrical ω-2θ scans are performed using the Bragg-Brentano geometry in a parallel beam set-up with an X-ray mirror in the incident beam and a parallel plate collimator in the diffracted beam side. High-resolution XRD and rocking curve measurements are performed with a hybrid X-ray mirror and a two-bounce Ge monochromator on the incident beam side and a 4-mm receiving slit on the diffracted beam side. For all these XRD measurements, samples are aligned with respect to the (006) peak of the c-cut Al_2O_3 substrate. The FE properties of the samples are measured using a parallel-plate configuration with a stainless steel rod (anode) having a flat circular base of 1.5 mm in diameter adjusted to a 300 μm distance from the sample (cathode) at a base pressure of 5×10^{-6} Torr. Voltage is swept using a computer-controlled Canberra power supply, and the current is measured using a Keithley 196 digital multimeter.

RESULTS AND DISCUSSION

Morphologies of the TO seed layer, GNI catalysts, and nanowires at different stages of growth, envisioned by using a mask-induced growth gradient technique described elsewhere,[14] are shown in Figure 1. The TO seed layer obtained on an Al_2O_3(0001) substrate by PLD at 650–700 °C exhibits a granular morphology (Figure 1(a)) with a 100–400 nm thickness. Our recent work shows that without the TO seed layer, CPLD growth of TO on a Al_2O_3(0001) substrate leads to randomly oriented nanowires.[14] The presence of this seed layer is therefore important, because the seed layer provides not only a perfectly lattice-matched substrate with good thermal uniformity upon radiative heating for the growth of vertically aligned nanowires, but also a conductive path for the emission current. A seed layer thickness of 100 nm or more is required, because it can be deposited reproducibly using the PLD method and its conductivity becomes thickness-independent above this thickness.[15] The stress in the interfacial layer of the film due to its lattice mismatch with the substrate is also fully relaxed over the 100 nm or more thickness range to provide a perfect lattice match for epitaxial growth. The Au film sputter-coated on the granular TO seed layer forms particulate GNIs, upon annealing at 500 °C (Figure 1(b)). Depositing TO on the so-obtained GNI/TO seed layer template at 500 °C in an Ar atmosphere leads to vapor–liquid–solid growth of TO nanowires with the gold catalysts on top (Figure 1(c)). Nanowires are found to be predominantly grown in parallel to one another and perpendicular to the TO seed layer (Figure 1(c)). A very few of the nanowires appear to grow at an acute angle with respect to the substrate (Figure 1(c), inset: marked by arrows). This inclined growth occurs most likely due to the growth in the [101] direction that makes an acute angle, ~33.93°, with respect to the [100] growth direction of the seed layer, which will be addressed further below in our XRD analysis. Upon further deposition, both perpendicular and inclined nanowires grow in length (Figure 1(d)) till to such point that the inclined nanowires cannot extend further in length due to spatial blockage and perpendicular nanowire growth dominates uniformly all over the substrate (Figures 1(e)–1(g)). The as-grown vertically aligned nanowires have a nearly square cross-section with a side length of 60–90 nm, which depends on the GNI size. The length of the nanowires is found to be 1–15 μm and is mainly dependent on the deposition time (40–60 min) and deposition rate, with the latter influenced by the target-to-substrate distance (40–50 mm).

Figures 2(a) and 2(b) show the local crystalline structure of a typical nanowire representative of several samples examined by TEM. The low-resolution TEM image (Figure 2(a)) depicts the uniform crystalline structure of the nanowire with thickness variation at the edges causing the observed differences in contrast, while the high-resolution TEM image (Figure 2(b)) shows nearly perfect single crystalline structure of the nanowire with no detectable

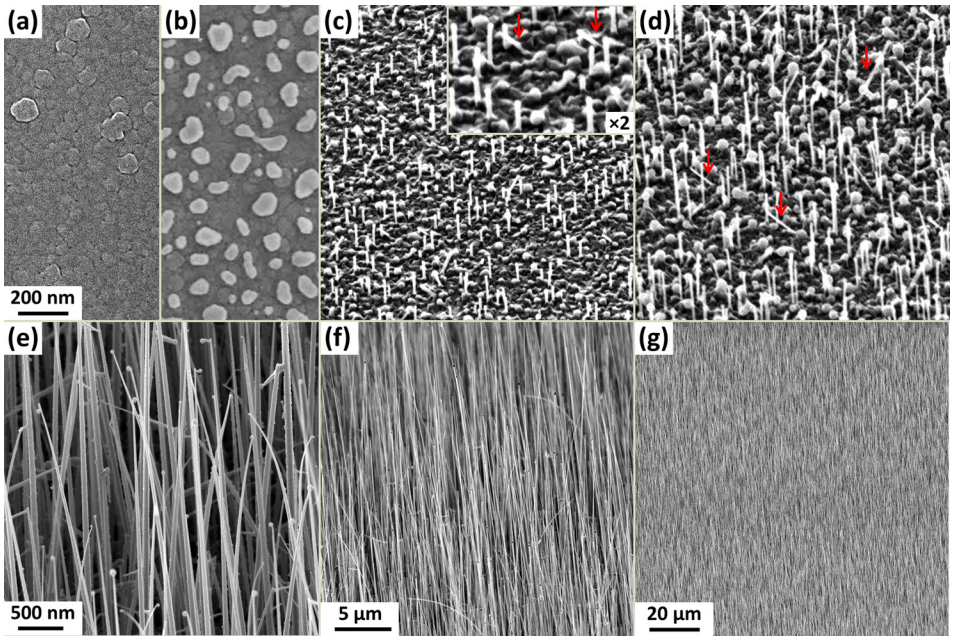

FIG. 1. Helium ion microscopy images of the samples at different stages of deposition leading to nanowire growth on a c-cut Al_2O_3 substrate: (a) tin dioxide seed layer growth at 750 °C in O_2, (b) gold nanoisland catalysts prepared by sputter-coating a thin gold film on the tin dioxide seed layer followed by annealing at 500 °C, (c) initial stage of nanowire growth at 500 °C in Ar, (d) progress in the nanowire growth leading to longer nanowires [(b) to (d) share the 200 nm scale bar of (a)], (e) to (g) final morphology of nanowires obtained after 60 min deposition at different magnifications.

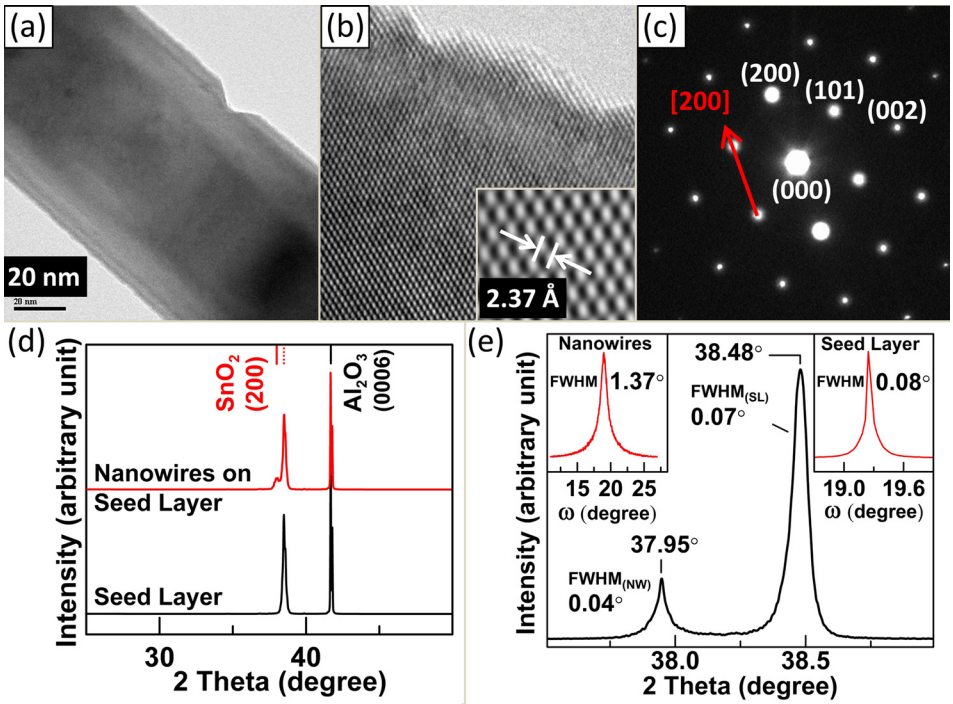

FIG. 2. TEM images of nanowires collected at (a) low resolution, and (b) high resolution, with the lattice spacing shown in inset, and (c) an indexed selected area electron diffraction pattern with the growth direction marked by arrow. (d) Symmetrical XRD scan for tin dioxide seed layer and for nanowires on the seed layer; and (e) high-resolution XRD pattern on (200) peak of nanowires on seed layer and the rocking curves of the (200) peaks associated with the nanowires (top left inset) and the seed layer (top right inset).

amorphous layer on the edges. The 2.37 ± 0.05 Å spacing between atomic planes in the growth direction of the nanowire reveals a [200] growth direction (Figure 2(b), inset). Figure 2(c) shows the indexed single crystalline selected area electron diffraction (SAED) pattern collected at a lower magnification with the aperture covering the entire width of the nanowire shown in Figure 2(a). This SAED pattern shows the single crystallinity of the structure across the nanowire width and confirms the [200] growth axis of the nanowire (marked by an arrow in Figure 2(c)) with side surfaces of (010) and (101) for the nanowire under study.

The average crystalline structures of the seed layer without and with the deposited nanowires are also examined by using XRD, and the results are shown in Figures 2(d) and 2(e). Symmetrical XRD results (Figure 2(d)) exhibit only a single (200) peak for the TO seed layer at $38.48 \pm 0.02°$, which is shifted 0.53° with respect to the peak position reported in the reference pattern of tin dioxide (37.950° in PDF2 #00-041-1445). In spite of the good lattice match between $Al_2O_3(0001)$ and $SnO_2(200)$, this minor shift in the peak position could be due to the difference in the surface structure of $Al_2O_3(0001)$ and $SnO_2(200)$. In particular, $Al_2O_3(0001)$ has a rhombus unit cell with a lattice constant of 4.7588 Å (PDF2 #00-042-1468), while $SnO_2(200)$ has a rectangle unit cell with lattice parameters of 4.7382 Å and 3.1871 Å (PDF2 #00-041-1445). The XRD pattern of the nanowires obtained by a 60-min deposition on the seed layer also shows only the (200) peak, which appears as a shoulder on the lower 2θ side of the (200) peak of the TO seed layer. In order to resolve these two (200) peaks, XRD pattern of the nanowire sample is measured using a monochromated high-resolution configuration (Figure 2(e)). It is evident that the new (200) peak corresponding to the nanowires has restored to its strain-free position (37.950°), as expected for the free-standing nanowires grown in microns away from the substrate. Furthermore, to investigate the spread in the alignment of nanowires on the film, rocking curve measurement is performed on the (200) peaks of the seed layer and the nanowires (Figure 2(e), insets). Though the nanowires are found to have a larger FWHM of 1.37° in comparison to that of the seed layer, 0.08°, the observed FWHM for the nanowires is discernibly small. This is indicative of the remarkably small variation in the vertical alignment of nanowires over their ultra-long average length of 15 μm (with respect to the substrate), especially in spite of their high mechanical flexibility.

The so-obtained TO NWs are especially suitable for FE applications, because a high aspect ratio with a sharp apex and aligned growth can typically enhance the emission properties. Examining their FE properties shows that the TO NW arrays exhibit a great FE performance in spite of the poor conductivity of the pristine TO seed layer as the back contact. Figure 3(a) shows the FE current density (J) as a function of electric field (E) for two typical nanowire samples with relatively short and long lengths. The short nanowire sample shown in Figure 3(b) is deposited with a target-to-substrate distance of 50 mm for 40 min leading to a low density of vertically aligned nanowires with $\sim$1 μm length (1 μm NW array), while the sample shown in Figure 3(c) is obtained with a smaller target-to-substrate distance of 40 mm for a longer duration of 60 min resulting in a high density of nanowires $\sim$15 μm in length (15 μm NW array). We observe turn-on fields of 3.0 V μm^{-1} and 3.8 V μm^{-1} at a current density of 1 μA cm^{-2} for the 15 μm and 1 μm NW arrays, respectively. These samples also show excellent FE stability as revealed by nearly identical FE curve obtained for 1st and 40th cycles (Figure 3(a)).

Previous studies[7,16,17] have shown that the turn-on field and field enhancement factor depend on the separation between the anode and cathode. Therefore, different anode-to-cathode separations and thresholds for the turn-on field

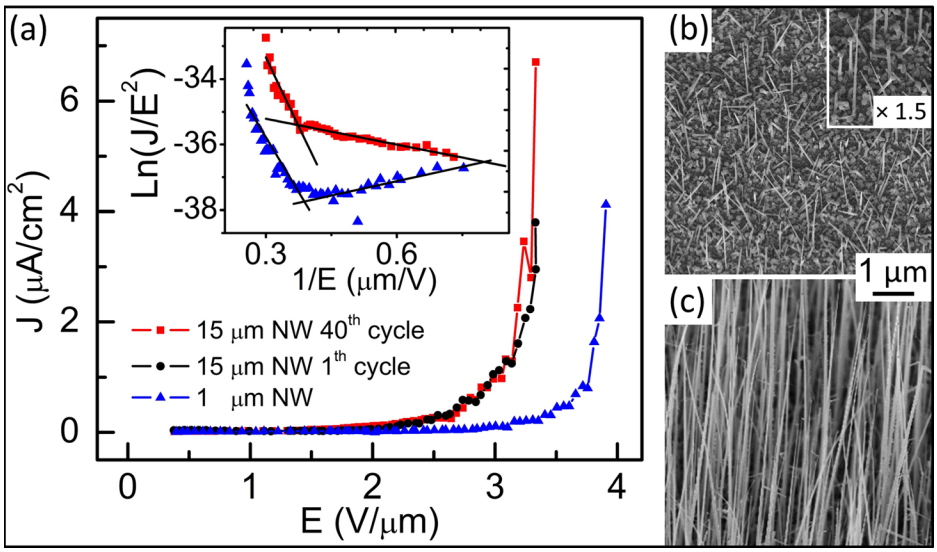

FIG. 3. (a) Current density (J) as a function of electric field (E) in a typical parallel plate field emission configuration and the corresponding Fowler-Nordheim plots (inset) for 1 and 15 μm NW samples, shown with the respective SEM images [collected with a 50° sample tilt], obtained by CPLD for (b) 40 min at a target-to-substrate separation of 50 mm, and (c) 90 min at a target-to-substrate separation of 40 mm. The J vs E curves obtained for over 40 V sweep cycles are remarkably similar.

from 0.1 to 10 μA cm^{-2} that have been employed in early studies on the FE properties of 1D TO nanostructures make the comparison of these data difficult. The turn-on fields obtained for the aligned nanowire samples in the present work are found to be discernibly lower than those reported by Zhang *et al.* (2.6–3.2 V μm^{-1} at 0.1 μA cm^{-2})[18] and He *et al.* (6.4–5.8 V μm^{-1} at 10 μA cm^{-2}),[8] and comparable to the lowest values reported (4.5–2.3 V μm^{-1} at 1 μA cm^{-2})[7] for pure 1D TO films. It should be noted that the lower turn-on fields of 1.5 and 1.6 V μm^{-1} reported, respectively, for Al-doped SnO_2 nanowires[19] and for SnO_2 nanorod film by co-evaporation of chloride salts of zinc and tin[20] are both likely due to doping effects and should not be compared with the present work (without any doping). Previous reports on the emission from single carbon nanotube emitters show that the field enhancement factor at the tip is directly proportional to the aspect ratio of the emitter, i.e., h/r for a cylinder of height h with a top hemisphere of radius r.[17,21] The lower turn-on field found for our 15 μm NW array can therefore be ascribed to their higher aspect ratio that gives rise to an increased field enhancement factor. The high aerial density of the nanowires could, however, introduce a screening effect, where the close proximity of the emitters reduces field penetration to the base and decreases the field enhancement factor in comparison to an individual well-isolated emitter.[22,23] The optimal density reported by Nilsson *et al.*[22] based on electrostatic calculations is 10^7 emitters cm^{-2}, which is much lower than the nearly 3×10^8 emitter cm^{-2} in our dense 15 μm NW array. In order to further analyze the FE behavior of these nanowire arrays, we show their Fowler-Nordheim (FN) plots (in the inset of Figure 3(a)) using the FN relation,[23] $J = \frac{A\beta^2E^2}{\phi}\exp(-\frac{B\phi^{\frac{3}{2}}}{\beta E})$, where J is the current density (A m^{-2}), E is the electric field (V m^{-1}), ϕ is the work function (eV), and A=1.54 $\times$ 10^{-6} A eV V^{-2} and B=6.83 $\times$ 10^9 eV$^{-3/2}$ V m^{-1}. Using a work function value of 4.7 eV, as reported for SnO_2,[24] the field enhancement factor due to the geometry of a nanowire array, β, can be obtained for the vertically aligned NWs from the slope of the FN plot. From the linear part of the FN plot (Figure 3(a), inset), we obtain a β value of 3.1×10^3 for the 1 μm NW array. Interestingly, for the 15 μm NW array, we observe two linear emission regimes, one with a β value of 2.5×10^3 at high field and the other one with a remarkably higher β value of 2.6×10^4 at lower field, where the 1 μm NW array does not emit. Not only are these β values observed for high-field emission (3.1×10^3, 2.5×10^3) among the highest values ever reported for SnO_2 nanowires [493.6 and 1402.9,[8] 460 to 2304,[7] 2866,[20] and 2280–1720 (Ref. 19)], the field enhancement factor measured for the low-field emission part of the 15 μm NW array (2.6×10^4) is also significantly higher than the reported values for SnO_2 and other oxide NW arrays, including vertically aligned catalyst-free ZnO nanowires (1500),[25] aligned Au-catalyzed ZnO nanobelts (1.4×10^4),[26] and Cu-catalyzed ZnO nanowire (7.2×10^3).[27]

In order to understand the observed difference in the FE behavior of 15 and 1 μm NW arrays and the remarkably high field enhancement factor of the 15 μm NW sample at low field, we examine the morphology of the samples after the FE experiments. While the 1 μm NW array does not show any detectable changes, the morphology of the 15 μm NW array is strongly affected by the FE experiment, as shown in Figure 4. The aligned morphology of the NW array (Figure 4(a)) is changed by formation of conical tipi structures that appear uniformly over the entire emitting area (Figure 4(b)). A closer examination of the NW array (Figure 4(c)) shows that the as-grown flexible, vertically aligned, ultra-long nanowires of the 15 μm NW array exhibit a narrow length distribution. These nanowires form two types of conical tipi structures (Figures 4(d) and 4(e)) after the FE measurement. In one type of these structures (Figure 4(d)), the catalysts in the form of a Sn-Au alloy, discussed in detail elsewhere,[14] located at the tip of nanowires fuse together and form a larger metal tip. In the other type (Figure 4(e)), nanowires twist around one another at the tip without formation of any large catalyst at the tip. Figures 4(f) and 4(g) show (the top views of) the morphological arrangements of the NW array before and after the FE measurement, respectively. The high mechanical flexibility of the nanowires is evident from the observed bent morphology near the tip for ultra-long

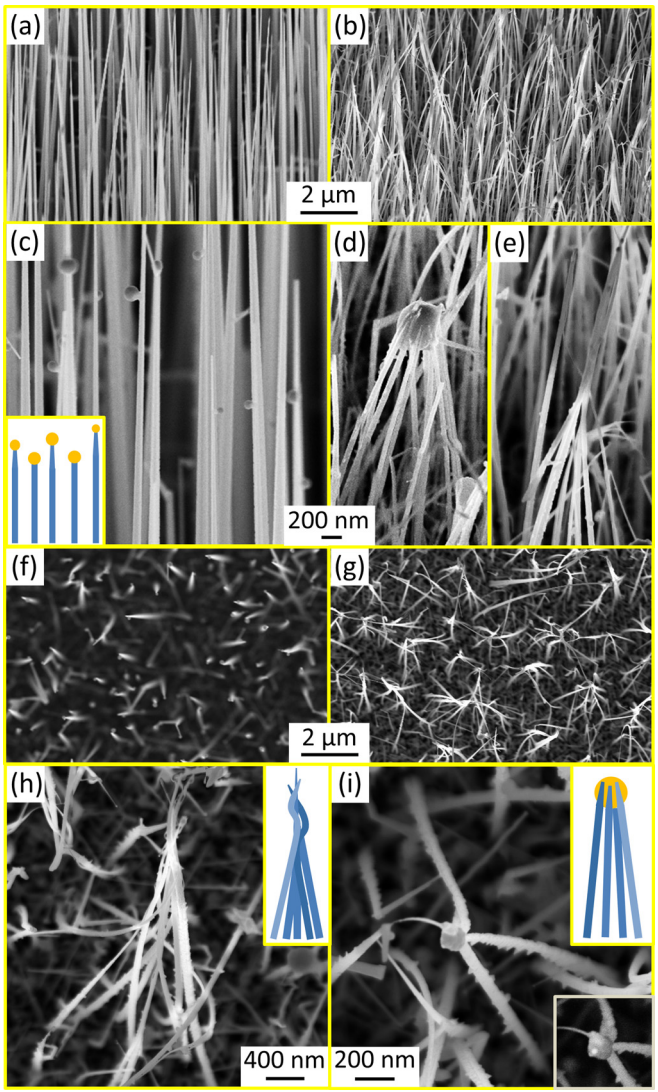

FIG. 4. SEM images, collected with (a)–(e) 50° sample tilt and (f)–(i) no sample tilt, of the 15 μm NW array (a), (c), and (f) before and (b), (d), (e), and (g)–(i) after the field emission measurement. Schematic models, shown as insets of (c), (h), and (i), illustrate the morphology of nanowires as-grown and the two possible reorganization arrangements observed after the field emission measurements, and the bottom right inset of (i) is the back-scattered SEM image of the tip. Images in each row share the same scale bar unless separate scale bars are shown.

nanowires (Figure 4(f)). After the FE measurement, conical structures appear to have formed uniformly over the emission area with an average base diameter of ca. 2 μm (Figure 4(g)). NWs with a slight difference in the length and NWs with lost catalyst tip tend to form the twisted conical morphology, shown in Figure 4(h) and illustrated in the schematics, while NWs with similar lengths prefer to form the conical morphology with a large catalyst tip, shown in Figure 4(i) along with the corresponding schematics. The observed contrast in the SEM image (obtained with a back-scattered electron detector) of the large catalyst tips formed after the FE measurement (Figure 4(i), bottom inset) suggests that the majority of the tip is made up of tin, while the catalyst tip of the as-grown NW is mainly gold with some Au-rich Au-Sn alloy as observed in our XRD results.[14] Formation of these tipi structures therefore occurs with possible chemical reduction of SnO_2 to Sn metal, leading to the attachment of the NWs and formation of larger catalysts by melted Sn metal. Mechanism that drives the formation of these structures is the attractive magnetic forces between the NWs within the observed proximity of ~1 μm radius during the FE process. Carrying parallel emission currents leads to the attraction of nanowires and the accompanying joule heating causes melting and fusion of the catalyst tip, in effect resulting in nano spot-welding at the nanowire tips. These self-reorganizations are found to occur after the first FE cycle, and no detectable change is observed upon further voltage cycling. These conical assemblies could greatly enhance the FE properties of the NW array, which would account for the observed improvement in the turn-on field and field enhancement factor of the NW array. By tilting the NWs into a conical geometry, the screening effect of the adjacent NWs is reduced, which leads to a better field penetration to the base of the NWs and therefore better field exposure of the entire NW length. In addition to the possible added contribution from emission of the entire NW length, formation of a single emission point in each tipi structure leads to well-separated emission tips and reduces the emitter aerial density approximately by an order of magnitude to 3×10^7 emitter cm^{-2} (as observed in our SEM images), which is in the optimal range based on the electrostatic calculation by Nilsson *et al.*[22] Due to the small differences in the work functions of tin (4.42 eV),[28] gold (4.83 eV),[29] and tin dioxide (4.7 eV),[24] changes in the composition of the catalyst are not expected to affect the β value significantly. Moreover, the observed increase in the catalyst size has an inverse effect on the aspect ratio and hence the field enhancement factor. Therefore, the observed changes in the size and composition of the catalyst cannot contribute to the observed enhanced FE properties.

CONCLUSIONS

In summary, vertically aligned SnO_2 nanowires are deposited using the CPLD method by pre-depositing a TO seed layer epitaxially along the [200] direction on a c-cut Al_2O_3 substrate. FE measurement on these nanowires yields a stable emission with a low turn-on field and a high field enhancement factor for both 1 and 15 μm NW arrays. Moreover, the 15 μm NW array, with a higher NW aerial density, exhibits a remarkably high field enhancement factor of 2.6×10^4 at low field. The improved FE behavior of the 15 μm NW array is attributed to the self-reorganization of nanowires to a conical tipi structure during the FE measurement, which leads to an optimum emitter density and a greatly enhanced field penetration to the base of the NW array. This self-reorganization is driven by magnetic attraction of NWs carrying parallel emission currents, which becomes significant and leads to the observed reorganization of dense, flexible, ultra-long nanowires with a narrow length distribution.

ACKNOWLEDGMENTS

The present work was supported by the Natural Sciences and Engineering Research Council of Canada.

[1]M. S. Arnold, P. Avouris, Z. W. Pan, and Z. L. Wang, J. Phys. Chem. B **107**, 659–663 (2003).
[2]Z. L. Wang, Annu. Rev. Phys. Chem. **55**, 159–1596 (2004).
[3]M. Law, D. J. Sirbuly, J. C. Johnson, J. Goldberger, R. J. Saykally, and P. Yang, Science **305**, 1269–1273 (2004).
[4]M. H. Huang, S. Mao, H. Feick, H. Yan, Y. Wu, H. Kind, E. Weber, R. Russo, and P. Yang, Science **292**, 1897–1899 (2001).
[5]N. S. Xu and S. E. Huq, Mater. Sci. Eng. R **48**, 47–189 (2005).
[6]Y. Cheng, P. Xiong, C. S. Yun, G. F. Strouse, J. P. Zheng, R. S. Yang, and Z. L. Wang, Nano Lett. **8**, 4179–4184 (2008).
[7]Y. J. Chen, Q. H. Li, Y. X. Liang, T. H. Wang, Q. Zhao, and D. P. Yu, Appl. Phys. Lett. **85**, 5682 (2004).
[8]J. H. He, T. H. Wu, C. Hsin, K. M. Li, L. J. Chen, Y. L. Chueh, L. J. Chou, and Z. L. Wang, Small **2**, 116–120 (2006).
[9]Z. R. Dai, J. L. Gole, J. D. Stout, and Z. L. Wang, J. Phys. Chem. B **106**, 1274–1279 (2002).
[10]S. Bazargan and K. T. Leung, J. Phys. Chem. C **116**, 5427–5434 (2012).
[11]J. Q. Hu, Y. Bando, Q. L. Liu, and D. Golberg, Adv. Funct. Mater. **13**, 493–496 (2003).
[12]Z. Liu, D. Zhang, S. Han, C. Li, T. Tang, W. Jin, X. Liu, B. Lei, and C. Zhou, Adv. Mater. **15**, 1754–1757 (2003).
[13]Z. R. Dai, Z. W. Pan, and Z. L. Wang, Solid State Commun. **118**, 351–354 (2001).
[14]S. Bazargan and K. T. Leung, J. Chem. Phys. **138**, 104704 (2013).
[15]A. Ivashchenko, I. Kerner, G. Kiosse, and I. Maronchuk, Thin Solid Films **303**, 292–294 (1997).
[16]Z. Xu, X. D. Bai, and E. G. Wang, Appl. Phys. Lett. **88**, 133107 (2006).
[17]C. J. Edgcombe and U. Valdre, J. Microsc. **203**, 188–194 (2001).
[18]Y. Zhang, K. Yu, G. Li, D. Peng, Q. Zhang, H. Hu, F. Xu, W. Bai, S. Ouyang, and Z. Zhu, Appl. Surf. Sci. **253**, 792–796 (2006).
[19]L. A. Ma, Y. Ye, L. Q. Hu, K. L. Zheng, and T. L. Guo, Physica E **40**, 3127–3130 (2008).
[20]X. Wang, W. Liu, H. Yang, X. Li, N. Li, R. Shi, H. Zhao, and J. Yu, Acta Mater. **59**, 1291–1299 (2011).
[21]J.-M. Bonard, K. Dean, B. Coll, and C. Klinke, Phys. Rev. Lett. **89**, 2–5 (2002).
[22]L. Nilsson, O. Groening, C. Emmenegger, O. Kuettel, E. Schaller, L. Schlapbach, H. Kind, J.-M. Bonard, and K. Kern, Appl. Phys. Lett. **76**, 2071 (2000).
[23]J.-M. Bonard, N. Weiss, H. Kind, T. Stöckli, L. Forró, and K. Kern, Adv. Mater. **13**, 184–188 (2001).
[24]T. Minami, T. Miyata, and T. Yamamoto, Surf. Coat.Technol. **108–109**, 583–587 (1998).
[25]H. Ham, G. Shen, J. H. Cho, T. J. Lee, S. H. Seo, and C. J. Lee, Chem. Phys. Lett. **404**, 69–73 (2005).
[26]W. Z. Wang, B. Q. Zeng, J. Yang, B. Poudel, J. Y. Huang, M. J. Naughton, and Z. F. Ren, Adv. Mater. **18**, 3275–3278 (2006).
[27]S. Y. Li, P. Lin, C. Y. Lee, and T. Y. Tseng, J. Appl. Phys. **95**, 3711 (2004).
[28]J. G. Simmons, Phys. Rev. Lett. **10**, 10–12 (1963).
[29]P. Anderson, Phys. Rev. **115**, 553–554 (1959).